Geophysical Research Letters

RESEARCH LETTER
10.1029/2025GL116498

Frictional Behavior of the Southern San Andreas Fault Reveals Ability to Host Shallow Slow Slip Events

A. A. DiMonte[1], A. K. Ault[1], S. Shreedharan[1], and G. Hirth[2]

[1]Department of Geosciences, Utah State University, Logan, UT, USA, [2]Department of Earth, Environment, and Planetary Sciences, Brown University, Providence, RI, USA

Key Points:

- Experiments on southern San Andreas fault gouge indicate low friction, transitional frictional behavior, and low (<0.001/decade) healing
- We show overlap of experimental healing and stress drop values with those derived from geodetic observations of shallow slow slip events (SSEs)
- San Andreas fault gouge could host shallow SSEs and localize shallow earthquake rupture propagation

Supporting Information:

Supporting Information may be found in the online version of this article.

Correspondence to:

A. A. DiMonte,
alex.dimonte@usu.edu

Citation:

DiMonte, A. A., Ault, A. K., Shreedharan, S., & Hirth, G. (2025). Frictional behavior of the southern San Andreas fault reveals ability to host shallow slow slip events. *Geophysical Research Letters*, *52*, e2025GL116498. https://doi.org/10.1029/2025GL116498

Received 16 APR 2025
Accepted 6 JUN 2025

Author Contributions:

Conceptualization: A. A. DiMonte, A. K. Ault, S. Shreedharan, G. Hirth
Data curation: A. A. DiMonte
Formal analysis: A. A. DiMonte
Funding acquisition: A. K. Ault, S. Shreedharan, G. Hirth
Investigation: A. A. DiMonte
Methodology: A. A. DiMonte, S. Shreedharan
Project administration: A. K. Ault
Resources: A. K. Ault, S. Shreedharan
Software: S. Shreedharan
Supervision: A. K. Ault
Visualization: A. A. DiMonte
Writing – original draft: A. A. DiMonte

Abstract The southern San Andreas fault is in its interseismic period, occasionally releasing some stored elastic strain during triggered slow slip events (SSEs) at <2.5 km depth. A distinct, shallowly exhumed gouge defines the fault and is present at SSE depths. To evaluate if this material can host SSEs, we characterize its mineralogy, microstructures, and frictional behavior with water-saturated deformation experiments near-in situ conditions, and we compare laboratory healing rates to natural SSEs. Our results show that slip localizes along clay surfaces in both laboratory and natural settings. The gouge is weak (coefficient of friction of ∼0.29), exhibits low healing rates (<0.001/decade), and transitions from unstable to stable behavior at slip rates above ∼1 μm/s. Healing rate and friction drop data from laboratory instabilities are comparable to geodetically-constrained values for SSEs. Collective observations indicate this gouge could host shallow SSEs and/or localize slip facilitating dynamic rupture propagation to the surface.

Plain Language Summary The southern San Andreas fault is likely overdue for an earthquake, but it experiences transient slip without releasing seismic energy. To understand this behavior, we characterize the composition, textures, and friction of the near-surface fault rocks. We performed experiments on powdered fault gouge, collected from the San Andreas fault, which inform how the friction changes as a function of velocity. A fault that lacks the ability to restrengthen, or heal, in between events and weaken with increasing velocity could promote transient aseismic behavior. The San Andreas fault gouge is weak and does not heal. It also weakens at plate tectonic slip rates but begins to strengthen at rates similar to velocities associated with transient aseismic fault slip. These observations, together with comparisons to geodetic observations of transient slip, imply the gouge should not nucleate shallow earthquakes but can host transient aseismic slip.

1. Introduction

Slow slip events (SSEs) are one mode of fault slip that releases some portion of stored strain energy along shallow depths of strike-slip faults (e.g., Bürgmann, 2018; Neyrinck et al., 2024). Complexities in fault geometry may influence slip mode (Lee et al., 2024), but the frictional properties of shallow faults potentially promote SSEs (Wei et al., 2013). Strike-slip faults that comprise the North American plate boundary in southern California, including the southern San Andreas (SSAF), Superstition Hills, and Imperial faults, host shallow (<3 km), spontaneous or triggered SSEs (Goulty et al., 1978; Parker et al., 2021; Tymofyeyeva et al., 2019; Wei et al., 2011). Recent geodetic studies characterize the pulse-like rupture of 2023 SSEs along the Superstition Hills and Imperial faults in unprecedented spatial and temporal detail (Materna et al., 2024; Vavra et al., 2024), highlighting an opportunity to better understand the mechanisms behind shallow SSE nucleation, propagation, and arrest.

The Coachella Valley section of the SSAF, extending from Indio Hills to Bombay Beach, CA (Figure 1a) experiences shallow SSEs. The long-term tectonic slip rate of the SSAF is ∼14–20 mm/yr (Behr et al., 2010; Blanton et al., 2020; Sieh, 1986; Tong et al., 2014), which is partitioned into a shallow creep rate of 2–4 mm/yr (Lindsey et al., 2014; Sieh and Williams, 1990), triggered SSEs, and coseismic slip. The 2010 El Mayor Cucapah and 2017 Chiapas earthquakes triggered SSEs along the SSAF resulting in 4–25 mm of slip in the upper ∼2.5 km of the fault zone observed geodetically and with creepmeters (Figure 1b; Parker et al., 2021; Tymofyeyeva et al., 2019).

The main trace of the SSAF is delineated by a distinct, phacoid-bearing "red clay" gouge that extends to depths of ∼3 km (Figure 1c; Ajala et al., 2019; Babcock, 1974; Bergh et al., 2019; Bürgmann, 1991; Fuis et al., 2017). The

Writing – review & editing:
A. A. DiMonte, A. K. Ault,
S. Shreedharan, G. Hirth

specific composition (mineralogy, clay content) of this gouge is not known. The presence of this material along the surface trace of the SSAF and at the depths of SSEs (Parker et al., 2021; Tymofyeyeva et al., 2019) presents a unique opportunity to evaluate whether the "red clay" gouge promotes nucleation and/or propagation of shallow SSEs.

Here we characterize the frictional behavior of exhumed SSAF gouge in Mecca Hills, CA (Figure 1c) using deformation experiments at near-in situ conditions paired with mineralogical and microstructural analyses. Mineralogy imparts a strong control on fault strength and healing (Carpenter et al., 2016; Tesei et al., 2012). Healing, or interseismic shear strength recovery, is required for repeated earthquakes along a fault, and can be quantified experimentally (Dieterich, 1972; Marone and Saffer, 2015). Weak faults with low frictional healing rates are characterized by creep, SSEs, or frequent, small (low stress drop) earthquakes (Carpenter et al., 2011; Shreedharan et al., 2023). Laboratory SSEs emerge near the frictional stability boundary at plate-driving rates (nm/s) and disappear at typical experimental rates (>1 μm/s) that are too fast for realistic healing mechanisms (Eijsink & Ikari, 2022; Ikari & Kopf, 2017), highlighting the utility of implementing plate-driving rates to accurately assess frictional behavior. We compare experimentally derived parameters of frictional healing and stress drop to those estimated from natural SSEs and use field and experimental observations to assess the ability of this "red clay" gouge to host SSEs along the shallow SSAF.

2. The Southern San Andreas Fault in Mecca Hills

Exhumed structures along the Coachella Valley section provide access to fault materials that experienced deformation at shallow depths in the past. Because the SSAF dips ~50–70° to the NE (Fuis et al., 2017; Vavra et al., 2023), broad zones of transpression and associated uplift occur along the SSAF in Indio Hills, Mecca Hills, and Durmid Hill (Figure 1; Bürgmann, 1991; Fattaruso et al., 2014; Jänecke et al., 2018). In the Mecca Hills, deformation is distributed along the "red clay" gouge of the main SSAF and in a series of subparallel faults, including the Skeleton Canyon and Painted Canyon faults, which likely converge with the dipping SSAF at depth in a flower-like structure (Figure 1c; Bergh et al., 2019; Sylvester & Smith, 1976). Gouge-rich fault cores of the Painted Canyon fault zone dissect exhumed Precambrian to Late Cretaceous crystalline basement (DiMonte et al., 2022; Moser et al., 2017, 2021), and foliated, clay-bearing gouge of the Skeleton Canyon fault developed in mudstones of the overlying Plio-Pleistocene Palm Spring Formation (Bergh et al., 2019; McNabb et al., 2017). Models of surface displacements along the main SSAF in Mecca Hills from the post-2017 Chiapas earthquake SSE suggests slip occurred at a depth of ~0.5 ± 0.1 km (Tymofyeyeva et al., 2019). At 0.5 km depth, the SSAF dissects sedimentary rock (Ajala et al., 2019), indicating that exhumed sediment-hosted SSAF gouge is likely representative of the fault material present at depths where these SSEs occur.

3. Materials and Methods

We observed and sampled ($n = 15$) the phacoid-bearing SSAF gouge at four locations between Painted Canyon and Box Canyon in Mecca Hills (Figure 1c). Semi-quantitative X-ray diffraction (XRD) was used to characterize the mineralogy of bulk and clay-sized (<2 μm) fractions of each sample (Text S1; Table S1 in Supporting Information S1; Data Set S1, https://doi.org/10.6084/m9.figshare.27165414.v5). We selected sample DSA20-1 for deformation experiments because its bulk clay content (29%) is representative of the mean from all samples (27%). The gouge is dominated by a fine-grained matrix, so >1 cm-diameter phacoids were removed from experimental aliquots. Powdered gouge was sieved to <36 μm and <125 μm size fractions yielding similar minimum and mean grain size distributions (Text S1; Figures S1–S3 in Supporting Information S1).

Powdered gouge of sample DSA20-1 was deformed using a direct shear apparatus (Figure S4 in Supporting Information S1) in USU's Rock Deformation and Earthquake Mechanics Lab (Tables S2–S4 in Supporting Information S1). Slide-hold-slide (SHS) and velocity-step tests quantify healing rates and the rate-and-state frictional stability parameter (a-b), respectively (Beeler et al., 1994). Positive a-b values indicate velocity strengthening behavior that promotes stable fault slip; negative a-b values indicate velocity weakening behavior, a condition for the onset of unstable slip (Scholz, 2019). In the rate-and-state framework, sliding stability also depends on healing (e.g., Dieterich, 1979) and the stiffness (k) of the fault surroundings or loading system. When k is less than a critical value,

$$k_c = \sigma_{\text{eff}}(b - a)/D_c \quad (1)$$

10.1029/2025GL116498

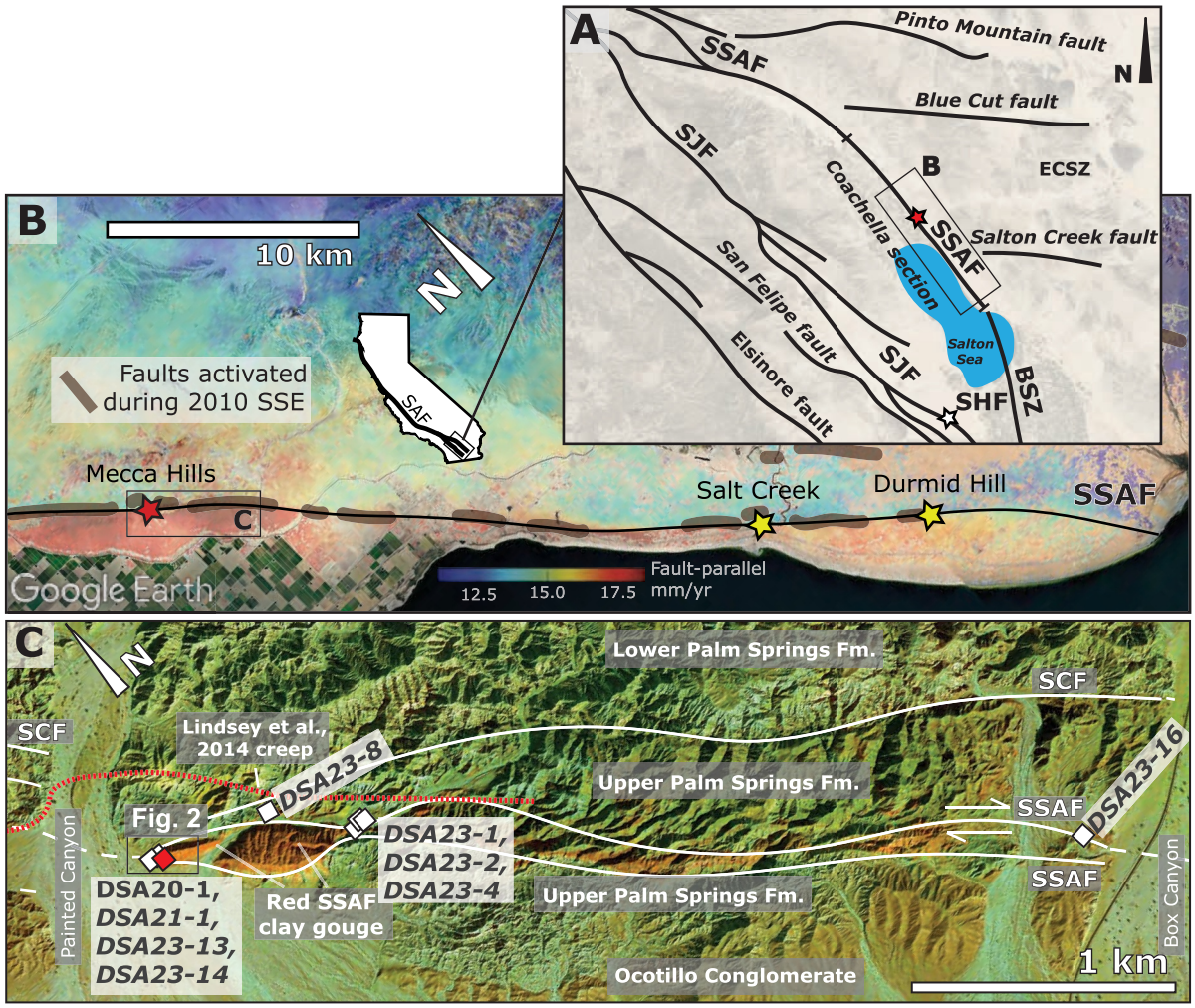

Figure 1. (a) Map showing fault traces in southern California including SSAF, San Jacinto fault (SJF), Brawley Seismic Zone (BSZ), and Superstition Hills fault (SHF). Starred locations host shallow slow slip event (SSE). (b) Google Earth imagery with SSAF, our field (red star) and other (yellow stars) locations with SSAF gouge, fault-parallel surface velocities from InSAR (adapted from Lindsey et al., 2014), and fault traces activated during SSE following 2010 El Mayor Cucapah earthquake (brown; adapted from Parker et al., 2021). (c) False-color Google Earth image with SSAF and Skeleton Canyon fault (SCF) in Mecca Hills showing "red clay" gouge, with sample locations (squares) and trace of fault creep from InSAR (red dashed line; Lindsey et al., 2014).

where σ_{eff} is effective normal stress and D_c is critical slip distance, instability and stick-slip occurs (Gu et al., 1984; Ruina, 1983).

Experiments were designed to approximate conditions at depths of <1 km where SSAF gouge deforms at depth today. Experiments were conducted at room temperature, 10 MPa effective stress, and room humidity (20%–21% relative humidity; experiments DS024, DS034) or in deionized water-saturated conditions (experiments DS045, DS046) using gouge sieved to <36 μm (DS024) or <125 μm (DS034, DS045, DS046). Saturated samples were held at 10 MPa for 11 hr prior to shear to ensure saturation when frictional parameters were determined (cf. Ikari, 2019; Shreedharan et al., 2022; Text S2; Figure S5 and S6 in Supporting Information S1). All experiments involved an initial run-in of 6 mm to ensure fabric development (cf. Haines et al., 2013). The run-in was followed by SHS tests with holds of 10–10,000s and 1 μm/s slip between holds and then a sequence of velocity steps initiating at 5 nm/s with order of magnitude velocity increases up to 5 μm/s. Natural and experimental slip surfaces from sample DS20-1 were imaged with a scanning electron microscope (SEM) to characterize and compare microstructures. See Text S2 in Supporting Information S1 for detailed experimental protocols and Text S3 in Supporting Information S1 for SEM sample preparation and operating conditions.

The coefficient of friction (μ) is calculated as

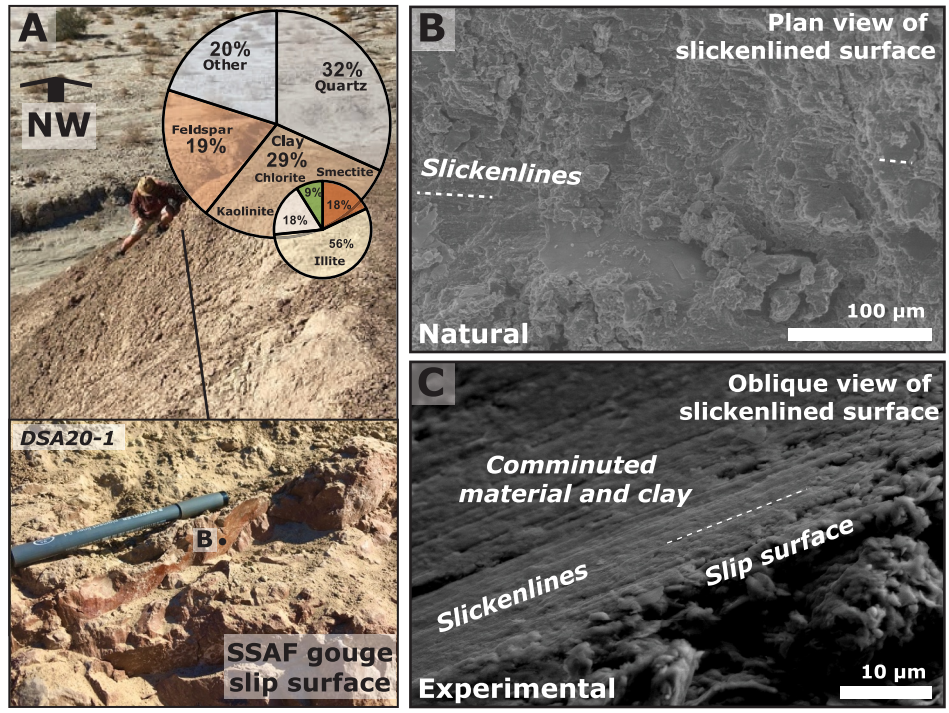

Figure 2. (a) Exposure of sample DSA20-1 with insets of slip surfaces and X-ray diffraction results. Black dot denotes location of (b) SEM images of slickenlined slip surfaces from natural sample DSA20-1 and (c) generated during experiment DS046.

$$\mu = \tau/\sigma_{\text{eff}}, \tag{2}$$

where τ is shear stress. Healing ($\Delta\mu$) is estimated by subtracting the steady state coefficient of friction (μ_{ss}) before a hold from the peak coefficient of friction (μ_s) following a hold (Text S2 in Supporting Information S1)

$$\Delta\mu = \mu_s - \mu_{ss}. \tag{3}$$

$$\frac{d(\mu_{ss})}{\ln(V)} \tag{4}$$

Healing rate, β (/decade), is approximated as $\Delta\mu$/log(t). a-b was estimated in two ways: graphically from Equation 4 (Beeler et al., 1994), and values of a, b, D_c, k were inverted using both the Aging and Slip law fits in RSFit3000 (Text S2 in Supporting Information S1; Skarbek & Savage, 2019). We calculated the recurrence interval and stress drop ($\Delta\tau$) of stick-slip events for each experiment that exhibited stick-slip behavior at a given velocity by selecting two individual events that were visually representative of the range of $\Delta\tau$ for the step.

4. Results

4.1. Field, Composition, and Microstructural Observations of Natural SSAF Gouge

New field observations show the "red clay" gouge is ubiquitous along the SSAF in Mecca Hills (Figure 1c). The SSAF is locally expressed as map-scale west verging thrusts and folds, with subsidiary fault zones that merge into the main SSAF (cf. Bergh et al., 2019). Subvertical fold limbs have axial-planar, foliated clay slip surfaces (mm- to cm-scale) with strike-slip slickenlines (Figure S7a in Supporting Information S1). Indurated fault surfaces (up to m-scale), oriented parallel and oblique to the SSAF trace, display horizontal and subvertical slickenlines (Figure 2a). Gouge layers vary from gray to tan, maroon, and red-orange (Figure S7b in Supporting Information S1). Within ~5 m of gouge-rich faults, the Upper Palm Spring Formation sandstone is weakly consolidated, bleached, and/or exhibits deformation bands, but distal sandstone is fractured in open folds.

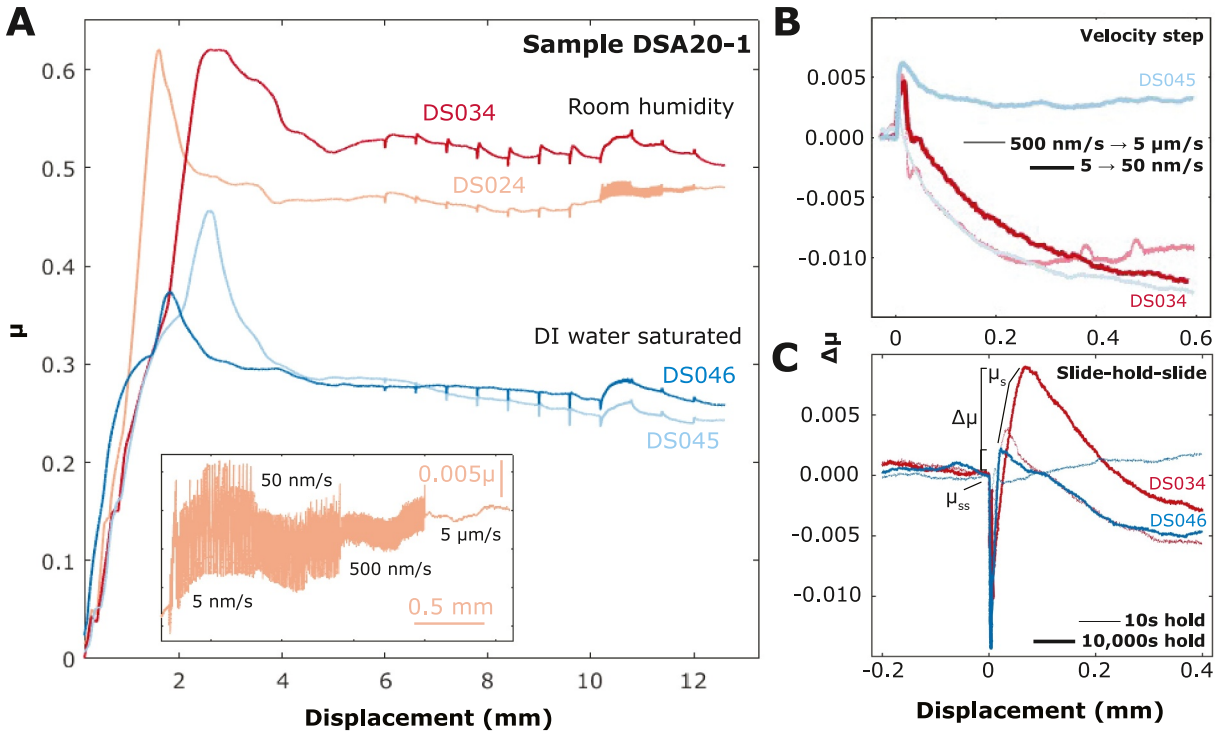

Figure 3. (a) Coefficient of friction (μ) evolution over displacement for room humidity (red, salmon) and water-saturated (dark, light blue) experiments. Inset: stick-slip behavior in experiment DS024. (b) Representative velocity steps for experiments DS034 and DS045. (c) Representative SHS results for experiments DS034 and DS046, where μ_{ss} and μ_s are friction before and peak after specific holds, and $\Delta\mu$ (noted with brackets) is the difference.

The mean modal composition (±1σ standard deviation) of the 15 gouge samples from bulk XRD is 36 ± 11% quartz, 27 ± 12% clay, 14 ± 13% plagioclase, 10 ± 4% calcite, 9 ± 3% K-feldspar, and additional minor (<2%) phases (Table S1 in Supporting Information S1). The mean clay composition is ~49 ± 8% illite, 26 ± 11% smectite, 14 ± 7% kaolinite, 11 ± 6% chlorite. Mineralogic variability (σ/mean) reflects either true compositional heterogeneity in the gouge and phacoids due to their provenance or error related to the semi-quantitative nature of the analysis. Sample DSA20-1 approximates the mean bulk values, and the <2 μm size fraction indicates the clay is 56% illite, 18% kaolinite, 18% smectite, and 9% chlorite (Figure 2a).

SEM images reveal the gouge comprises many undulating, parallel and oblique slip surfaces with slickenlines (Figure 2b, Figure S8 in Supporting Information S1). Fine (sub-μm), wispy, clay platelets are aligned or form clumps that occur with larger broken grains of quartz and feldspar. Some phacoids are enveloped by clay layers (Figure S8 in Supporting Information S1).

4.2. Experimental Results

We discuss data from room humidity experiments (DS024, DS034) and experiments that reached complete saturation prior to shear (DS045, DS046) and include results from experiments informing the saturation time in Table S2 in Supporting Information S1. Room humidity gouge has a residual or μ_{ss} of 0.50 ± 0.03 (average ± standard deviation) at 4 mm displacement; saturated gouge has a significantly lower μ_{ss} of 0.29 ± 0.01 (Figure 3a).

We report the frictional stability parameter a-b as the average ± 1σ standard deviation of values estimated from Equation 4 and RSFit3000 inversions (Text S2; Table S5; Figure S9 in Supporting Information S1). Experiment DS024 exhibited stick-slip instabilities at velocities <5 μm/s, indicating that a-b is negative at these lower sliding rates, but numerical values were not estimated due to the difficulty in resolving μ_{ss} during stick-slips (Figure 3a, Figure S10 in Supporting Information S1). Data from experiment DS034 shows a-b of room humidity gouge is constant and negative (−0.0050 to −0.0042) across the tested velocities (Figure 3b). The a-b of saturated gouge

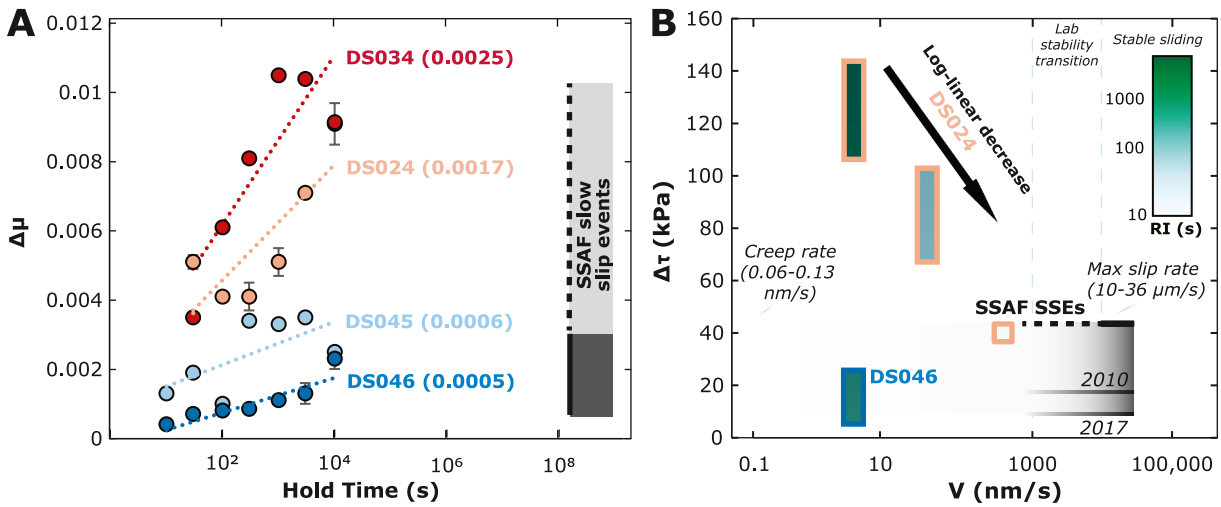

Figure 4. (a) $\Delta\mu$ as a function of hold time for each experiment with β (parentheses). Light and dark gray boxes denote range and average, respectively, of $\Delta\mu$ estimated from slow slip events (SSEs) triggered along local (5–10 km) southern San Andreas (SSAF) intervals from El Mayor Cucapah (Parker et al., 2021) and Chiapas (Tymofyeyeva et al., 2019) earthquakes. (b) Range of $\Delta\tau$ of stick slip events observed during experiments and SSEs in nature over local (~5–10 km) SSAF segments (gray box, lines are averages) as a function of velocity; green color gradient is recurrence interval; blue dashed lines delineate laboratory stability transition velocities.

increases with increasing load-point velocity, indicating a transition from velocity weakening to velocity strengthening behavior at rates near 0.5–10 μm/s (Figure 3b, Figure S11 in Supporting Information S1).

The magnitude of $\Delta\mu$ and β decrease with water-saturated conditions (Figure 4a, Figure S12; Table S6 in Supporting Information S1). Frictional healing across experiments exhibits a log-linear increase with time over the range of investigated hold times (cf. Carpenter et al., 2016). Room humidity gouge has a β of 0.0017–0.0025; saturated gouge has a β of 0.0005–0.0006. Inaudible and periodic stick slip instabilities occurred at 5–500 nm/s loading rates in experiment DS024 (Figure S13a in Supporting Information S1), as well as at 5 nm/s during saturated experiment DS046. DS046 also displayed period multiplying behavior, or repeat stress drops with lower periods that recur quasiperiodically between "regular" events (e.g., Mei et al., 2021; Figure S13b in Supporting Information S1). The $\Delta\tau$ and recurrence interval for stick slips decrease linearly as a function of the log of the imposed slip velocity for room-humidity experiment DS024 (Figure 4b; Table S7, Figure S14 in Supporting Information S1; $\Delta\tau$ = 140–40 kPa, recurrence interval of 3,000–10 s).

During each experiment, the gouge developed a localized and composite slip-surface with sub-mm-spaced slickenlines parallel to the slip direction. SEM images from saturated experiment DS046 reveal that slickenlined surfaces are defined by aligned clay platelets (<μm in length) and comminuted quartz and feldspar (Figure 2c, Figure S15 in Supporting Information S1).

5. Discussion

5.1. SSAF Gouge Is Weak and Localizes Slip

The low friction of saturated SSAF gouge is controlled by (a) its clay content, (b) fabric development in clay, and (c) the specific phyllosilicate mineralogy. Although the gouge is dominated by silicates, and its clay content is only 29%, clay exerts an outsized control on fault strength. The gouge is also significantly weaker when water-saturated (Figure 3a), consistent with prior work on clay-bearing gouge (Crawford et al., 2008; Ikari et al., 2007; Moore & Lockner, 2007). Our friction values are similar to or lower than those from natural and synthetic gouge powders with >50% clay (Carpenter et al., 2016; Ikari, 2019; Ikari & Kopf, 2017; Saffer & Marone, 2003) and overlap values of 30% clay with associated slip localization in clay (Wojatschke et al., 2016). The specific clays in the SSAF gouge impart a second order effect on the friction, and minor compositional and grain size differences between experiments could explain intersample variability in μ_{ss} at room humidity. Although the <2 μm size fraction of sample DSA20-1 is dominated by non-swelling clays (83% in total), 18% swelling smectite lowers the μ_{ss} beyond what is expected for mixtures comprising only non-swelling clays (Tembe et al., 2010).

The frictionally weak gouge localized slip along the SSAF. Similarly, in experiments, slickenlines developed on slip surfaces defined by clay platelets that envelop comminuted quartz and feldspar (Figure 2c). The development of these clay surfaces promotes slip localization and controls the friction (cf., Bedford et al., 2022; Wojatschke et al., 2016). The natural samples from the SSAF also exhibit striated and foliated clay slip surfaces that locally mantle stronger phacoids (Figures 2a and 2b, Figures S7 and S8 in Supporting Information S1). In contrast to the fault gouge, adjacent sandstone lacks structural evidence of significant shear. We suggest the contrasting mechanical behavior of gouge and sandstone or phacoids reinforces slip localization and strain accommodation in the weaker SSAF gouge (e.g., Smeraglia et al., 2017) over multiple spatial scales and earthquake cycles.

5.2. Ability of SSAF Gouge to Host Shallow SSEs

Experimental observations, and comparisons of experiments with data encoded in geodetically observed SSEs, support that the SSAF gouge can host shallow SSEs. First, our experiments were conducted at conditions that span the stability transition from stick slip to stable sliding. Water-saturated gouge exhibits a transition from velocity weakening to velocity strengthening frictional behavior at rates above 0.5–10 μm/s, potentially due to dilatant hardening (Figure S11 in Supporting Information S1; e.g., Shreedharan et al., 2022). Accounting for the timescales of pore water diffusion suggests that the observed frictional behavior is not strongly influenced by transient changes in pore fluid pressure during velocity steps or healing (Text S4 in Supporting Information S1).

Second, documented ultra-low healing rates for saturated SSAF gouge (Figure 4a) also promote stable creep or SSEs (Carpenter et al., 2012, 2015; Shreedharan et al., 2023). Prior work indicates that rotation and alignment of clay plates leads to saturation of the real area of contact and thus reduces interseismic healing (Bos & Spiers, 2000; Seyler et al., 2023).

Third, inaudible stick slip and slow slip behavior with small stress drops (<30 kPa) occurred at near-tectonic slip rates (5 nm/s) in one saturated experiment, consistent with prior work at plate rates and low normal stresses (Eijsink & Ikari, 2022; Ikari, 2019; Ikari & Kopf, 2017). Stick slip instabilities at loading rates up to 500 nm/s in one room humidity experiment exhibit a log-linear decrease in $\Delta\tau$ and recurrence interval at higher loading rates (Figure 4b). This negative correlation is likely controlled by a decrease in healing (Dieterich, 1979) and associated stability transition at higher velocities (Leeman et al., 2018). SSEs could also be promoted by a velocity dependent critical slip distance (D_c) reflecting gouge structural evolution (e.g., Shreedharan et al., 2022). Observed period-multiplying behavior indicates the gouge is close to the frictional stability transition, a condition conducive to laboratory SSEs or stick slip events with inaudible, slow strain release (Figure S13; Table S5 in Supporting Information S1; $k \sim k_c$; Barbot, 2019; Gu et al., 1984; Ikari, 2019; Leeman et al., 2016, 2018; Mei et al., 2021; Ruina, 1983). Inter-sample variability in stick-slip behavior may reflect compositional and/or grain size differences producing slightly different stiffnesses above and below k_c. Stick-slips in experiment DS024 (<36 μm), but not DS034 (<125 μm), are consistent with prior work suggesting a limited, fine grain size distribution promotes instability (Bedford and Faulkner, 2021; Anthony & Marone, 2005). Thus, instabilities could nucleate in saturated gouge at tectonic slip rates but then transition to stable slip as the fault slip accelerates. This would halt the expansion of the instability in a location before it reaches the critical size required for earthquake nucleation (Im et al., 2020; Mclaskey & Yamashita, 2017) but potentially propagate pulse-like SSEs such as those observed geodetically (Materna et al., 2024).

Fourth, because the gouge is present at SSE depths in Mecca Hills, we compare observations from our SHS experiments and laboratory SSEs ($\Delta\mu$, β, $\Delta\tau$, recurrence interval) with values calculated from triggered SSEs (Parker et al., 2021; Tymofyeyeva et al., 2019). The time between all historical (i.e., 1968, 1979, 1986, 2010, 2017) triggered SSEs detected by creepmeters provides bounds (7–24 years) on the recurrence interval. High-resolution geodetic data from the 2010 and 2017 SSEs inform $\Delta\tau$, which we calculate as (Kanamori & Brodsky, 2004)

$$\Delta\tau = GD/\sqrt{A}. \quad (5)$$

where G is shear modulus, D is slip displacement, and A is fault area (fault length × depth). We consider inferred depth ranges from prior work (0.5–2.5 km), pore fluid to normal stress ratios of 0.4–0.9, observed 6.8–15 mm displacement per event, and activated fault lengths of 10–40 km (Parker et al., 2021; Tymofyeyeva et al., 2019).

Additional details, calculations including historical creepmeter-derived estimates of slip, and caveats regarding these comparisons such as scaling of stiffness, are presented in Text S5 in Supporting Information S1.

The healing of saturated gouge extrapolated to SSE timescales is broadly consistent with the $\Delta\mu$ (0.0005–0.0027, locally up to 0.0115) calculated for effective normal stresses (e.g., 3.75–37.5 MPa) at which recently triggered SSEs occur (Figure 4a). Similarly, the experimental $\Delta\tau$ observed for slow events is commensurate with those calculated from the SSEs (~10–44 kPa; Figure 4b). The peak SSE velocities (~10–36 μm/s; Tymofyeyeva et al., 2019) are also similar to the velocity at which slip transitions from unstable to stable sliding in the lab (~0.5–10 μm/s) (Figure 4b). The compatibility between laboratory healing and observed SSEs, together with documented frictional behavior, indicate that past SSEs likely nucleated in and released most of their energy within the SSAF gouge at 0.5–2.5 km depth and will continue to do so in the future.

5.3. Clay-Bearing Gouge Will Localize Future Coseismic Slip Along the SSAF

The SSAF accommodates a portion of its slip aseismically, but the fault poses significant seismic hazard. It has an average recurrence interval of ~180 years and last experienced a major surface rupturing earthquake >300 years ago (~1690 CE, Philibosian et al., 2011; Rockwell et al., 2022). The next earthquake is expected to yield surface displacements ≤4 m (Fialko, 2006; Scharer & Yule, 2020). Gouge along the main SSAF likely extends through sedimentary rocks into underlying crystalline basement (Fuis et al., 2017) where it is analogous to foliated gouge cores in the exhumed Painted Canyon fault in Mecca Hills. Regardless of rock type, fault gouge is comparatively weak and thus localizes slip during the along-strike and up-dip propagation of earthquakes that nucleate at depth. Our field and experimental data highlight that foliated gouge provides a throughgoing zone of weakness from depth to the near-surface. If a large earthquake ($M_w \sim 7$) nucleates at depth, the gouge will experience seismic slip rates at which dynamic weakening occurs, facilitating the localization of earthquake slip along strike and to the surface (Di Toro et al., 2011; Smeraglia et al., 2017).

6. Conclusions

Geodetic and creepmeter data along the SSAF have captured triggered shallow SSEs during the protracted interseismic period. The SSAF is delineated by a shallowly-exhumed distinct "red clay" gouge that exists at the depths where these events nucleate. Experimental and field-based observations demonstrate that, below the water table, saturated weak gouge could localize slip owing to its clay content, specific clay mineralogy, and fabric. The SSAF gouge exhibits velocity dependent frictional stability, <0.001/decade healing rates, and laboratory slow slip, as well as yields healing rate and friction drop compatible with the geodetically-observed triggered SSEs. All of these observations suggest the gouge, where present within the SSAF zone, could host the observed shallow SSEs or facilitate shallow rupture propagation during an earthquake that nucleates at depth.

Data Availability Statement

Information used to derive the interpretations and conclusions of this work are provided in the main text and Supporting Information S1. The Supporting Information S1 contains text related to methods, 15 Supporting figures, and 7 tables. The data and code to process data (DiMonte et al., 2024) are archived and freely available at figshare.com (https://doi.org/10.6084/m9.figshare.27165414.v5).

Acknowledgments
This work was supported by grants: NSF (EAR-2039727) and SCEC (22082, 23081) to Ault and Hirth, NSF (EAR-2420543) to Ault, Hirth, and Shreedharan, a USU SPARC to Ault, and USGS (G24AP00232) and NSF (EAR-2342125) to Shreedharan. This is SCEC contribution 14092. We thank Fen Ann Shen (USU) and Martin Pentrak (ISGS) for analytical support. We thank Kristina Okamoto, an anonymous reviewer, and Editor German Prieto for feedback that improved the manuscript.

References

Ajala, R., Persaud, P., Stock, J. M., Fuis, G. S., Hole, J. A., Goldman, M., & Scheirer, D. (2019). Three-dimensional basin and fault structure from a detailed seismic velocity model of Coachella Valley, Southern California. *Journal of Geophysical Research: Solid Earth*, *124*(5), 4728–4750. https://doi.org/10.1029/2018jb016260

Anthony, J. L., & Marone, C. (2005). Influence of particle characteristics on granular friction. *Journal of Geophysical Research*, *110*(B8). https://doi.org/10.1029/2004jb003399

Babcock, E. A. (1974). Geology of the northeast margin of the Salton Trough, Salton Sea, California. *Geological Society of America Bulletin*, *85*(3), 321–332. https://doi.org/10.1130/0016-7606(1974)85<321:gotnmo>2.0.co;2

Barbot, S. (2019). Slow-slip, slow earthquakes, period-two cycles, full and partial ruptures, and deterministic chaos in a single asperity fault. *Tectonophysics*, *768*, 228171. https://doi.org/10.1016/j.tecto.2019.228171

Bedford, J. D., Faulkner, D. R., & Lapusta, N. (2022). Fault rock heterogeneity can produce fault weakness and reduce fault stability. *Nature Communications*, *13*(1), 326. https://doi.org/10.1038/s41467-022-27998-2

Beeler, N. M., Tullis, T. E., & Weeks, J. D. (1994). The roles of time and displacement in the evolution effect in rock friction. *Geophysical Research Letters*, *21*(18), 1987–1990. https://doi.org/10.1029/94gl01599

Behr, W. M., Rood, D. H., Fletcher, K. E., Guzman, N., Finkel, R., Hanks, T. C., et al. (2010). Uncertainties in slip-rate estimates for the Mission Creek strand of the southern San Andreas fault at Biskra Palms Oasis, southern California. *Bulletin*, *122*(9–10), 1360–1377. https://doi.org/10.1130/b30020.1

Bergh, S. G., Sylvester, A. G., Damte, A., & Indrevær, K. (2019). Polyphase kinematic history of transpression along the Mecca Hills segment of the San Andreas fault, southern California. *Geosphere*, *15*(3), 901–934. https://doi.org/10.1130/ges02027.1

Blanton, C. M., Rockwell, T. K., Gontz, A., & Kelly, J. T. (2020). Refining the spatial and temporal signatures of creep and co-seismic slip along the southern San Andreas Fault using very high resolution UAS imagery and SfM-derived topography, Coachella Valley, California. *Geomorphology*, *357*, 107064. https://doi.org/10.1016/j.geomorph.2020.107064

Bos, B., & Spiers, C. J. (2000). Effect of phyllosilicates on fluid-assisted healing of gouge-bearing faults. *Earth and Planetary Science Letters*, *184*(1), 199–210. https://doi.org/10.1016/s0012-821x(00)00304-6

Bürgmann, R. (1991). Transpression along the southern san Andreas fault, Durmid Hill, California. *Tectonics*, *10*(6), 1152–1163. https://doi.org/10.1029/91tc01443

Bürgmann, R. (2018). The geophysics, geology and mechanics of slow fault slip. *Earth and Planetary Science Letters*, *495*, 112–134. https://doi.org/10.1016/j.epsl.2018.04.062

Carpenter, B. M., Ikari, M. J., & Marone, C. (2016). Laboratory observations of time-dependent frictional strengthening and stress relaxation in natural and synthetic fault gouges. *Journal of Geophysical Research: Solid Earth*, *121*(2), 1183–1201. https://doi.org/10.1002/2015jb012136

Carpenter, B. M., Marone, C., & Saffer, D. M. (2011). Weakness of the San Andreas Fault revealed by samples from the active fault zone. *Nature Geoscience*, *4*(4), 251–254. https://doi.org/10.1038/ngeo1089

Carpenter, B. M., Saffer, D. M., & Marone, C. (2012). Frictional properties and sliding stability of the San Andreas fault from deep drill core. *Geology*, *40*(8), 759–762. https://doi.org/10.1130/g33007.1

Carpenter, B. M., Saffer, D. M., & Marone, C. (2015). Frictional properties of the active San Andreas Fault at SAFOD: Implications for fault strength and slip behavior. *Journal of Geophysical Research: Solid Earth*, *120*(7), 5273–5289. https://doi.org/10.1002/2015jb011963

Chen, R., & Petersen, M. D. (2011). Probabilistic fault displacement hazards for the Southern San Andreas Fault using scenarios and empirical slips. *Earthquake Spectra*, *27*(2), 293–313. https://doi.org/10.1193/1.3574226

Crawford, B. R., Faulkner, D. R., & Rutter, E. H. (2008). Strength, porosity, and permeability development during hydrostatic and shear loading of synthetic quartz-clay fault gouge. *Journal of Geophysical Research*, *113*(B3). https://doi.org/10.1029/2006jb004634

Dieterich, J. H. (1972). Time-dependent friction in rocks. *Journal of Geophysical Research*, *77*(20), 3690–3697. https://doi.org/10.1029/jb077i020p03690

Dieterich, J. H. (1979). Modeling of rock friction: 1. Experimental results and constitutive equations. *Journal of Geophysical Research*, *84*(B5), 2161–2168. https://doi.org/10.1029/jb084ib05p02161

DiMonte, A., Ault, A., Shreedharan, S., Hirth, G., & Pentrak, M. P. (2024). Dataset for Frictional behavior of the shallow southern San Andreas fault reveals ability to host shallow slow slip events [Dataset]. *Figshare.com*. https://doi.org/10.6084/m9.figshare.27165414.v5

DiMonte, A. A., Ault, A. K., Hirth, G., & Bradbury, K. K. (2022). Hematite accommodated shallow, transient Pleistocene slow slip in the exhumed southern San Andreas fault system, California, USA. *Geology*, *50*(12), 1443–1447. https://doi.org/10.1130/g50489.1

Di Toro, G., Han, R., Hirose, T., De Paola, N., Nielsen, S., Mizoguchi, K., et al. (2011). Fault lubrication during earthquakes. *Nature*, *471*(7339), 494–498. https://doi.org/10.1038/nature09838

Eijsink, A. M., & Ikari, M. J. (2022). Plate-rate frictional behavior of sediment inputs to the Hikurangi subduction margin: How does lithology control slow slip events? *Geochemistry, Geophysics, Geosystems*, *23*(6), e2022GC010369. https://doi.org/10.1029/2022gc010369

Fattaruso, L. A., Cooke, M. L., & Dorsey, R. J. (2014). Sensitivity of uplift patterns to dip of the san Andreas fault in the Coachella Valley, California. *Geosphere*, *10*(6), 1235–1246. https://doi.org/10.1130/ges01050.1

Fialko, Y. (2006). Interseismic strain accumulation and the earthquake potential on the southern San Andreas fault system. *Nature*, *441*(7096), 968–971. https://doi.org/10.1038/nature04797

Fuis, G. S., Bauer, K., Goldman, M. R., Ryberg, T., Langenheim, V. E., Scheirer, D. S., et al. (2017). Subsurface geometry of the san Andreas fault in southern California: Results from the Salton Seismic Imaging Project (SSIP) and strong ground motion expectations. *Bulletin of the Seismological Society of America*, *107*(4), 1642–1662. https://doi.org/10.1785/0120160309

Gerstenberger, M. C., Marzocchi, W., Allen, T., Pagani, M., Adams, J., Danciu, L., et al. (2020). Probabilistic seismic hazard analysis at regional and national scales: State of the art and future challenges. *Reviews of Geophysics*, *58*(2), e2019RG000653. https://doi.org/10.1029/2019rg000653

Goulty, N. R., Burford, R. O., Allen, C. R., Gilman, R., Johnson, C. E., & Keller, R. P. (1978). Large creep events on the Imperial fault, California. *Bulletin of the Seismological Society of America*, *68*(2), 517–521. https://doi.org/10.1785/bssa0680020517

Gu, J.-C., Rice, J. R., Ruina, A. L., & Simon, T. T. (1984). Slip motion and stability of a single degree of freedom elastic system with rate and state dependent friction. *Journal of the Mechanics and Physics of Solids*, *32*(3), 167–196. https://doi.org/10.1016/0022-5096(84)90007-3

Haines, S. H., Kaproth, B., Marone, C., Saffer, D., & Van der Pluijm, B. (2013). Shear zones in clay-rich fault gouge: A laboratory study of fabric development and evolution. *Journal of Structural Geology*, *51*, 206–225. https://doi.org/10.1016/j.jsg.2013.01.002

Ikari, M. J. (2019). Laboratory slow slip events in natural geological materials. *Geophysical Journal International*, *218*(1), 354–387. https://doi.org/10.1093/gji/ggz143

Ikari, M. J., & Kopf, A. J. (2017). Seismic potential of weak, near-surface faults revealed at plate tectonic slip rates. *Science Advances*, *3*(11), e1701269. https://doi.org/10.1126/sciadv.1701269

Ikari, M. J., Saffer, D. M., & Marone, C. (2007). Effect of hydration state on the frictional properties of montmorillonite-based fault gouge. *Journal of Geophysical Research*, *112*(B6). https://doi.org/10.1029/2006jb004748

Im, K., Saffer, D., Marone, C., & Avouac, J.-P. (2020). Slip-rate-dependent friction as a universal mechanism for slow slip events. *Nature Geoscience*, *13*(10), 705–710. https://doi.org/10.1038/s41561-020-0627-9

Jänecke, S. U., Markowski, D. K., Evans, J. P., Persaud, P., & Kenney, M. (2018). Durmid ladder structure and its implications for the nucleation sites of the next M>7.5 earthquake on the San Andreas fault or Brawley seismic zone in southern California. *Lithosphere*, *10*(5), 602–631. https://doi.org/10.1130/l629.1

Jolivet, R., & Frank, W. B. (2020). The transient and intermittent nature of slow slip. *AGU Advances*, *1*(1), e2019AV000126. https://doi.org/10.1029/2019av000126

Kanamori, H., & Brodsky, E. E. (2004). The physics of earthquakes. *Reports on Progress in Physics*, *67*(8), 1429–1496. https://doi.org/10.1088/0034-4885/67/8/r03

Lee, J., Tsai, V. C., Hirth, G., Chatterjee, A., & Trugman, D. T. (2024). Fault-network geometry influences earthquake frictional behaviour. *Nature*, *631*(8019), 1–5. https://doi.org/10.1038/s41586-024-07518-6

Leeman, J. R., Marone, C., & Saffer, D. M. (2018). Frictional mechanics of slow earthquakes. *Journal of Geophysical Research: Solid Earth*, *123*(9), 7931–7949. https://doi.org/10.1029/2018jb015768

Leeman, J. R., Saffer, D. M., Scuderi, M. M., & Marone, C. (2016). Laboratory observations of slow earthquakes and the spectrum of tectonic fault slip modes. *Nature Communications*, *7*(1), 11104. https://doi.org/10.1038/ncomms11104

Lindsey, E. O., Fialko, Y., Bock, Y., Sandwell, D. T., & Bilham, R. (2014). Localized and distributed creep along the southern san Andreas fault. *Journal of Geophysical Research: Solid Earth*, *119*(10), 7909–7922. https://doi.org/10.1002/2014jb011275

Lockner, D. A., Morrow, C., Moore, D., & Hickman, S. (2011). Low strength of deep San Andreas fault gouge from SAFOD core. *Nature*, *472*(7341), 82–85. https://doi.org/10.1038/nature09927

Marone, C. (1998). Laboratory-derived friction laws and their application to seismic faulting. *Annual Review of Earth and Planetary Sciences*, *26*(1), 643–696. https://doi.org/10.1146/annurev.earth.26.1.643

Marone, C., & Saffer, D. M. (2015). The mechanics of frictional healing and slip instability during the seismic cycle. In *Earthquake seismology* (pp. 111–138). Elsevier Inc.

Materna, K., Bürgmann, R., Lindsay, D., Bilham, R., Herring, T., Crowell, B., & Szeliga, W. (2024). Shallow slow slip events in the Imperial Valley with along-strike propagation. *Geophysical Research Letters*, *51*(12), e2023GL108089. https://doi.org/10.1029/2023gl108089

Mclaskey, G. C., & Yamashita, F. (2017). Slow and fast ruptures on a laboratory fault controlled by loading characteristics. *Journal of Geophysical Research: Solid Earth*, *122*(5), 3719–3738. https://doi.org/10.1002/2016jb013681

McNabb, J. C., Dorsey, R. J., Housen, B. A., Dimitroff, C. W., & Messé, G. T. (2017). Stratigraphic record of Pliocene-Pleistocene basin evolution and deformation within the southern San Andreas fault zone, Mecca Hills, California. *Tectonophysics*, *719*, 66–85. https://doi.org/10.1016/j.tecto.2017.03.021

Mei, C., Barbot, S., & Wu, W. (2021). Period-Multiplying cycles at the transition between stick-slip and stable sliding and implications for the Parkfield period-doubling tremors. *Geophysical Research Letters*, *48*(7), e2020GL091807. https://doi.org/10.1029/2020gl091807

Moore, D. E., & Lockner, D. A. (2007). Friction of the smectite clay montmorillonite: A review and interpretation of data. *The Seismogenic Zone of Subduction Thrust Faults*, 317–345.

Moore, D. E., Lockner, D. A., & Hickman, S. (2016). Hydrothermal frictional strengths of rock and mineral samples relevant to the creeping section of the San Andreas Fault. *Journal of Structural Geology*, *89*, 153–167. https://doi.org/10.1016/j.jsg.2016.06.005

Moser, A. C., Ault, A. K., Stearns, M. A., Evans, J. P., & Guenthner, W. R. (2021). Late Oligocene–early Miocene detachment faulting in crystalline basement, Mecca Hills, CA, documented with zircon (U–Th)/He date-eU-visual radiation damage patterns. *Tectonics*, *40*(9), e2021TC006809.

Moser, A. C., Evans, J. P., Ault, A. K., Janecke, S. U., & Bradbury, K. K. (2017). (U–Th)/He thermochronometry reveals Pleistocene punctuated deformation and synkinematic hematite mineralization in the Mecca Hills, southernmost San Andreas Fault zone. *Earth and Planetary Science Letters*, *476*, 87–99. https://doi.org/10.1016/j.epsl.2017.07.039

Nevitt, J. M., Brooks, B. A., Catchings, R. D., Goldman, M. R., Ericksen, T. L., & Glennie, C. L. (2020). Mechanics of near-field deformation during co-and post-seismic shallow fault slip. *Scientific Reports*, *10*(1), 5031. https://doi.org/10.1038/s41598-020-61400-9

Neyrinck, E., Rousset, B., Doubre, C., Rivera, L., Lasserre, C., Doin, M.-P., et al. (2024). The slow slip event cycle along the Izmit segment of the North Anatolian Fault. *Earth and Planetary Science Letters*, *648*, 119104. https://doi.org/10.1016/j.epsl.2024.119104

Parker, J., Donnellan, A., Bilham, R., Ludwig, L. G., Wang, J., Pierce, M., et al. (2021). Buried aseismic slip and off-fault deformation on the southernmost San Andreas fault triggered by the 2010 El Mayor Cucapah earthquake revealed by UAVSAR. *Earth and Space Science*, *8*(8), e2021EA001682. https://doi.org/10.1029/2021ea001682

Philibosian, B., Fumal, T., & Weldon, R. (2011). San Andreas fault earthquake chronology and Lake Cahuilla history at Coachella, California. *Bulletin of the Seismological Society of America*, *101*(1), 13–38. https://doi.org/10.1785/0120100050

Rockwell, T. K., Meltzner, A. J., Haaker, E. C., & Madugo, D. (2022). The late holocene history of lake Cahuilla: Two thousand years of repeated fillings within the salton trough, imperial valley, California. *Quaternary Science Reviews*, *282*, 107456. https://doi.org/10.1016/j.quascirev.2022.107456

Roten, D., Olsen, K. B., Day, S. M., Cui, Y., & Fäh, D. (2014). Expected seismic shaking in Los Angeles reduced by San Andreas fault zone plasticity. *Geophysical Research Letters*, *41*(8), 2769–2777. https://doi.org/10.1002/2014gl059411

Ruina, A. (1983). Slip instability and state variable friction laws. *Journal of Geophysical Research*, *88*(B12), 10359–10370. https://doi.org/10.1029/jb088ib12p10359

Saffer, D. M., & Marone, C. (2003). Comparison of smectite-and illite-rich gouge frictional properties: Application to the updip limit of the seismogenic zone along subduction megathrusts. *Earth and Planetary Science Letters*, *215*(1–2), 219–235. https://doi.org/10.1016/s0012-821x(03)00424-2

Scharer, K. M., & Yule, D. (2020). A maximum rupture model for the southern San Andreas and San Jacinto faults, California, derived from paleoseismic earthquake ages: Observations and limitations. *Geophysical Research Letters*, *47*(15), e2020GL088532. https://doi.org/10.1029/2020gl088532

Scholz, C. H. (2019). *The mechanics of earthquakes and faulting*. Cambridge University Press.

Seyler, C. E., Shreedharan, S., Saffer, D. M., & Marone, C. (2023). The role of clay in limiting frictional healing in fault gouges. *Geophysical Research Letters*, *50*(20), e2023GL104984. https://doi.org/10.1029/2023gl104984

Shreedharan, S., Ikari, M., Wood, C., Saffer, D., Wallace, L., & Marone, C. (2022). Frictional and lithological controls on shallow slow slip at the northern Hikurangi margin. *Geochemistry, Geophysics, Geosystems*, *23*(2), e2021GC010107. https://doi.org/10.1029/2021gc010107

Shreedharan, S., Saffer, D., Wallace, L. M., & Williams, C. (2023). Ultralow frictional healing explains recurring slow slip events. *Science*, *379*(6633), 712–717. https://doi.org/10.1126/science.adf4930

Sieh, K. E. (1986). Slip rate across the San Andreas fault and prehistoric earthquakes at Indio, California. *Eos Trans. AGU*, *67*(44), 1200.

Sieh, K. E., & Williams, P. L. (1990). Behavior of the southernmost San Andreas fault during the past 300 years. *Journal of Geophysical Research*, *95*(B5), 6629–6645. https://doi.org/10.1029/jb095ib05p06629

Skarbek, R. M., & Savage, H. M. (2019). RSFit3000: A MATLAB GUI-based program for determining rate and state frictional parameters from experimental data. *Geosphere*, *15*(5), 1665–1676. https://doi.org/10.1130/ges02122.1

Smeraglia, L., Billi, A., Carminati, E., Cavallo, A., Di Toro, G., Spagnuolo, E., & Zorzi, F. (2017). Ultra-thin clay layers facilitate seismic slip in carbonate faults. *Scientific Reports*, *7*(1), 664. https://doi.org/10.1038/s41598-017-00717-4

Sylvester, A. G., & Smith, R. R. (1976). Tectonic transpression and basement-controlled deformation in San Andreas fault zone, Salton Trough, California. *AAPG Bulletin*, *60*(12), 2081–2102. https://doi.org/10.1306/c1ea3a73-16c9-11d7-8645000102c1865d

Tembe, S., Lockner, D. A., & Wong, T.-F. (2010). Effect of clay content and mineralogy on frictional sliding behavior of simulated gouges: Binary and ternary mixtures of quartz, illite, and montmorillonite. *Journal of Geophysical Research*, *115*(B3). https://doi.org/10.1029/2009jb006383

Tesei, T., Collettini, C., Carpenter, B. M., Viti, C., & Marone, C. (2012). Frictional strength and healing behavior of phyllosilicate-rich faults. *Journal of Geophysical Research*, *117*(B9). https://doi.org/10.1029/2012jb009204

Tong, X., Smith-Konter, B., & Sandwell, D. T. (2014). Is there a discrepancy between geological and geodetic slip rates along the San Andreas Fault System? *Journal of Geophysical Research: Solid Earth*, *119*(3), 2518–2538. https://doi.org/10.1002/2013jb010765

Tymofyeyeva, E., Fialko, Y., Jiang, J., Xu, X., Sandwell, D., Bilham, R., et al. (2019). Slow slip event on the Southern San Andreas fault triggered by the 2017 M w 8.2 Chiapas (Mexico) earthquake. *Journal of Geophysical Research: Solid Earth*, *124*(9), 9956–9975. https://doi.org/10.1029/2018jb016765

Vavra, E. J., Fialko, Y., Rockwell, T., Bilham, R., Štěpančíková, P., Stemberk, J., et al. (2024). Characteristic slow-slip events on the superstition Hills fault, southern California. *Geophysical Research Letters*, *51*(12), e2023GL107244. https://doi.org/10.1029/2023gl107244

Vavra, E. J., Qiu, H., Chi, B., Share, P.-E., Allam, A., Morzfeld, M., et al. (2023). Active dipping interface of the Southern San Andreas fault revealed by space geodetic and seismic imaging. *Journal of Geophysical Research: Solid Earth*, *128*(11), e2023JB026811. https://doi.org/10.1029/2023jb026811

Wei, M., Kaneko, Y., Liu, Y., & McGuire, J. J. (2013). Episodic fault creep events in California controlled by shallow frictional heterogeneity. *Nature Geoscience*, *6*(7), 566–570. https://doi.org/10.1038/ngeo1835

Wei, M., Sandwell, D., Fialko, Y., & Bilham, R. (2011). Slip on faults in the imperial valley triggered by the 4 april 2010 Mw 7.2 El mayor-cucapah earthquake revealed by InSAR. *Geophysical Research Letters*, *38*(1). https://doi.org/10.1029/2010gl045235

Wojatschke, J., Scuderi, M. M., Warr, L. N., Carpenter, B. M., Saffer, D., & Marone, C. (2016). Experimental constraints on the relationship between clay abundance, clay fabric, and frictional behavior for the C entral D eforming Z one of the S an A ndreas F ault. *Geochemistry, Geophysics, Geosystems*, *17*(10), 3865–3881. https://doi.org/10.1002/2016gc006500

References From the Supporting Information

Fulton, P. M., & Saffer, D. M. (2009). Potential role of mantle-derived fluids in weakening the San Andreas Fault. *Journal of Geophysical Research*, *114*(B7). https://doi.org/10.1029/2008jb006087

Ikari, M. J., Saffer, D. M., & Marone, C. (2009). Frictional and hydrologic properties of clay-rich fault gouge. *Journal of Geophysical Research*, *114*(B5). https://doi.org/10.1029/2008jb006089

Jeppson, T. N., & Tobin, H. J. (2015). San Andreas fault zone velocity structure at SAFOD at core, log, and seismic scales. *Journal of Geophysical Research: Solid Earth*, *120*(7), 4983–4997. https://doi.org/10.1002/2015jb012043

Samuelson, J., Elsworth, D., & Marone, C. (2009). Shear-induced dilatancy of fluid-saturated faults: Experiment and theory. *Journal of Geophysical Research*, *114*(B12). https://doi.org/10.1029/2008jb006273

Williams, P. L., McGill, S. F., Sieh, K. E., Allen, C. R., & Louie, J. N. (1988). Triggered slip along the San Andreas fault after the 8 July 1986 North Palm Springs earthquake. *Bulletin of the Seismological Society of America*, *78*(3), 1112–1122. https://doi.org/10.1785/bssa0780031112